Optical and Quantum Communications

Academic and Research Staff
Professor Jeffrey H. Shapiro, Dr. Franco N. C. Wong, Dr. Marco Fiorentino,
Dr. Vittorio Giovannetti, Dr. Friedrich König, Dr. Lorenzo Maccone

Graduate Students
Marius A. Albota, Baris I. Erkmen, Pavel V. Gorelik, Saikat Guha, Taehyun Kim,
Christopher E. Kuklewicz, Onur Kuzucu, Mohsen Razavi, Brent J. Yen

The central theme of our programs has been to advance the understanding of optical and quantum communication, radar, and sensing systems. Broadly speaking, this has entailed: (1) developing system-analytic models for important propagation, detection, and communication scenarios; (2) using these models to derive the fundamental limits on system performance; and (3) identifying, and establishing through experimentation the feasibility of, techniques and devices which can be used to approach these performance limits.

1. Quantum Information and Communication

Sponsors
Air Force Research Laboratory - Cooperative Agreement F30602-01-2-0546
Army Research Office - Grant DAAD-19-00-1-0177
Army Research Office - Grant DAAD-19-01-1-0647
Office of Naval Research - Contract N00014-03-1-0869
Office of Naval Research - Contract N00014-02-1-0717

Project Staff
Professor Jeffrey H. Shapiro, Dr. Franco N. C. Wong, Dr. Marco Fiorentino,
Dr. Vittorio Giovannetti, Dr. Friedrich König, Dr. Lorenzo Maccone, Marius A. Albota,
Pavel V. Gorelik, Saikat Guha, Taehyun Kim, Christopher E. Kuklewicz, Onur Kuzucu,
Mohsen Razavi, Brent J. Yen

We are embarked on research in the area of quantum information technology whose goal is to enable the quantum-mechanical information transmission, storage, and processing needed for future applications in quantum computing and quantum communication. Our theoretical work in this area has focused on architectural designs for long-distance teleportation and multi-party entanglement transmission, and on novel applications of entanglement. Of particular interest has been the identification of high-performance means for generating the polarization-entangled photons needed for many quantum information applications, including teleportation, entanglement-based quantum positioning and clock synchronization, and quantum secret sharing. Our main experimental work is focused on generation and application of entanglement sources with high brightness and wavelength tunability. In addition, we are interested in novel entanglement sources and their applications in enhanced quantum measurements and quantum teleportation protocols.

Architectural Analysis The preeminent obstacle to the development of quantum information technology is the difficulty of transmitting quantum information over noisy and lossy quantum communication channels, recovering and refreshing the quantum information that is received, and then storing it in a reliable quantum memory. We lead a team of researchers from MIT and Northwestern University (NU) that has proposed, analyzed, and is developing the key technological elements of a novel architecture for the singlet-state approach to quantum teleportation [1]. A simple block diagram of this architecture is shown in Fig. 1. It consists of an ultrabright narrowband source of polarization-entangled photons pairs (*P*), connected to a pair of

trapped Rb atom quantum memories (*M*) by transmission through *L*-km-long lengths of standard telecommunication fiber.

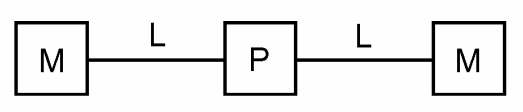

Figure 1. Schematic of long-distance quantum communication system: *P* = ultrabright narrowband source of polarization-entangled photon pairs; *L* = *L* km of standard telecommunication fiber; *M* = trapped atom quantum memory.

Each *M* block in Fig. 1 is a quantum memory in which a single ultracold ^{87}Rb atom is confined by a CO_2-laser trap in an ultra-high vacuum chamber with cryogenic walls within a high-finesse single-ended optical cavity. An abstract representation of the relevant hyperfine levels for such a memory is given in Fig. 2(a). A 795 nm photon in an arbitrary polarization can be absorbed, transferring the qubit from the photon to the degenerate *B* levels of Fig. 2(a), and thence to long-lived storage levels, by coherently driving the *B*-to-*D* transitions. By means of optically-off-resonant (OOR) transitions, the Bell states of two atoms in a single vacuum-chamber trap can be converted into superposition states of one of the atoms. All four Bell measurements needed for the Bennett *et al*. singlet-state teleportation process [2] can then be made, sequentially, by detecting the presence (or absence) of fluorescence as an appropriate sequence of OOR laser pulses is applied to the latter atom. The Bell-measurement results (two bits of classical information) in one memory can be sent to a distant memory, where (at most) two additional OOR pulses are needed to complete the state transformation process. More details on this memory, and its use in teleportation, are given in [3].

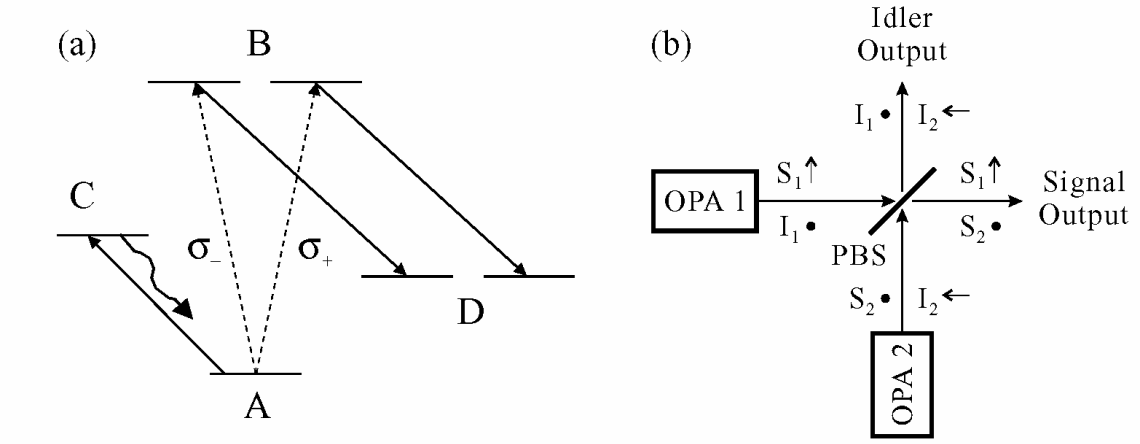

Figure 2. Essential components of singlet-state quantum communication system from Fig. 1. Left (a), simplified atomic-level schematic of the trapped Rb atom quantum memory: *A*-to-*B* transition occurs when one photon from an entangled pair is absorbed; *B*-to-*D* transition is coherently driven to enable storage in the long-lived *D* levels; *A*-to-*C* cycling transition permits nondestructive determination of when a photon has been absorbed. Right (b), ultrabright narrowband source of polarization-entangled photon pairs: each optical parametric amplifier (OPA1 and OPA2) is type-II phase matched; for each optical beam the propagation direction is *z*, and *x* and *y* polarizations are denoted by arrows and bullets, respectively; PBS, polarizing beam splitter.

The *P* block in Fig. 1 is an ultrabright narrowband source of polarization-entangled photon pairs [4], capable of producing ~10^6 pairs/sec in ~30 MHz bandwidth by appropriately combining the signal and idler output beams from two doubly-resonant type-II phase matched optical parametric

amplifiers (OPAs), as sketched in Fig. 2(b). The importance of our resonant approach to entanglement generation is the need to achieve high flux within the narrow linewidth of the Rb atom memory; existing parametric downconverter sources of entanglement are far too broadband to permit useful transmission rates in the Fig. 1 architecture.

During the past year we have augmented and generalized our performance analysis for the preceding teleportation architecture by examining the sensitivity of teleportation throughput and fidelity to imperfections in the source of polarization-entangled photons, and to errors in the polarization restoration system that follows fiber-optic propagation of these entangled photons. From our single-photon-error, cold-cavity loading analysis for the trapped Rb atom quantum memories [5,6], see Fig. 3, we have derived [7] the conditional joint density operator, given no erasure, that accounts for pump phase, gain, and detuning errors in a dual-OPA entanglement source, and for imperfect polarization restoration. We then evaluated the degradations of throughput and fidelity that result from these error mechanisms.

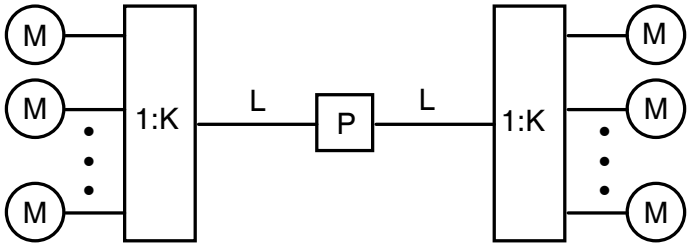

Figure 3. Notional scheme for converting single-photon memory loading errors into erasures. Each single-atom memory block in Fig.1 is replaced with a 1:*K* fan-out and *K* single-atom memories. A loading event is declared only when exactly one memory at each end of the fiber links has absorbed a photon. All other possibilities are erasures. A single-photon error occurs when a loading event does not store the singlet state that is desired for the teleportation application.

Figure 4 shows the impact of polarization restoration errors, θ_S and θ_I. As shown in these figures, imperfect polarization acts as a loss, viz., the throughput degrades dramatically as these error angles increase, but the teleportation fidelity remains high. More importantly, Fig. 4 shows that the requirements on polarization restoration to stay near peak throughput are not unduly severe.

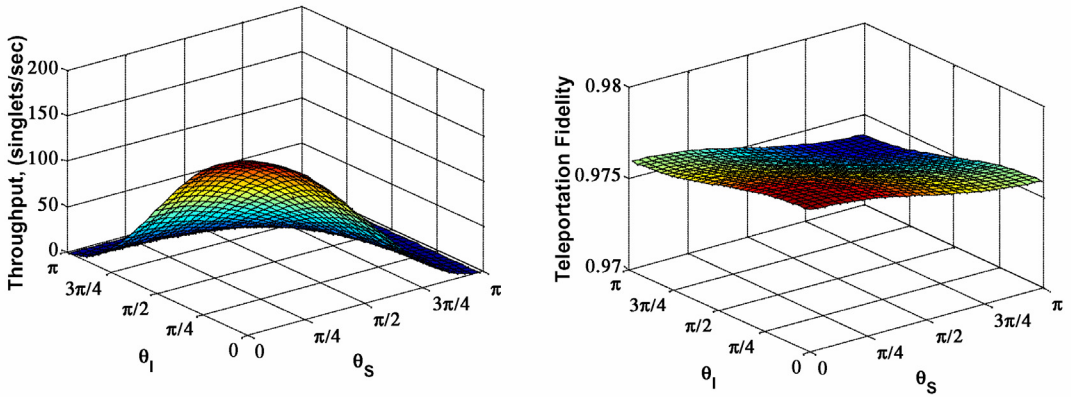

Figure 4. Left: throughput versus polarization-restoration error angles. Right: teleportation fidelity versus polarization-restoration error angles. These plots assume the OPAs operate at 1% of oscillation threshold, 2 dB/km fiber loss, 5 dB excess loss in each source-to-memory link, source-to-memory path length *L* = 25 km, and 500 kHz cycling rate for the loading protocol.

Figure 5 shows the consequence of a pump-phase error $\Delta\psi$ on teleportation fidelity. When $\Delta\psi$ = 0, the dual-OPA source has anti-phased pumps that produce the singlet state which is assumed in the teleportation protocol. When $\Delta\psi = \pi$, the dual-OPA source has in-phase pumps that

produce a triplet state. As shown in Fig.5, the unintended occurrence of the triplet state has a dramatic effect on teleportation fidelity. However, as shown in this figure, only modest pump-phase control is needed to maintain high-fidelity operation.

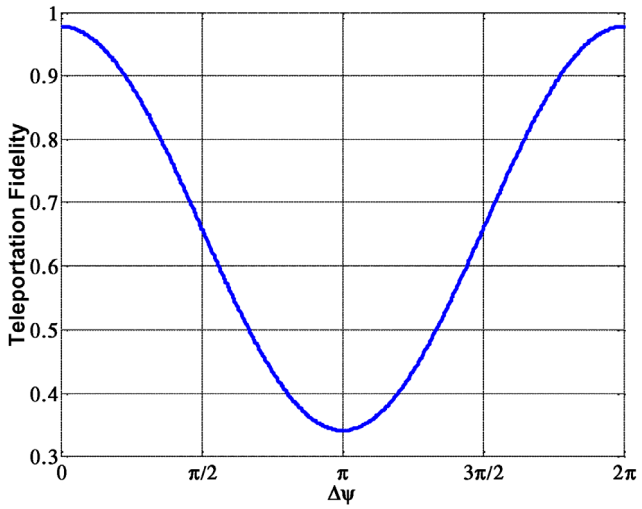

Figure 5. Teleportation fidelity versus dual-OPA pump-phase error. This plot assumes the OPAs operate at 1% of oscillation threshold, 2 dB/km fiber loss, 5 dB excess loss in each source-to-memory link, and source-to-memory path length L = 25 km.

Figure 6 quantifies the loss that is incurred in teleportation fidelity because of pump power fluctuations in the dual-OPA system. Each OPA is presumed to have an average gain that is 1% of oscillation threshold, but the gains themselves are independent, identically distributed, Gaussian random variables with variance σ^2_G. Because $\sigma^2_G = 10^{-4}$ corresponds to 1% pump-power fluctuations, we see that OPA gain fluctuations do not pose a major threat to teleportation fidelity.

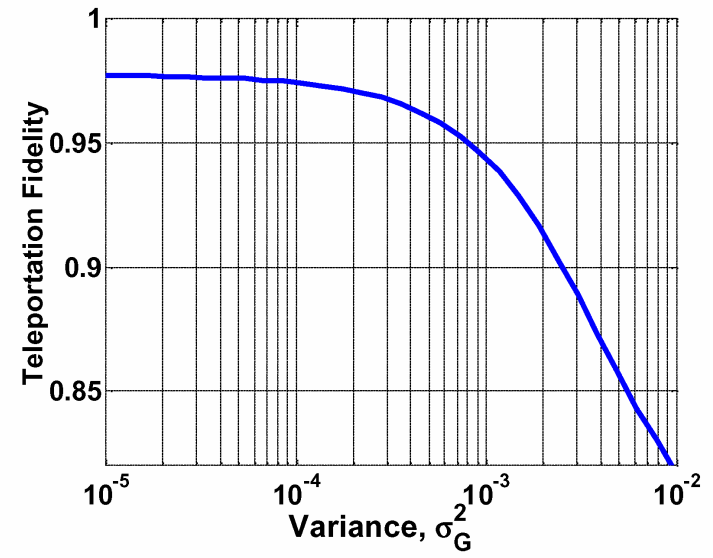

Figure 6. Teleportation fidelity versus dual-OPA pump-gain variance. This plot assumes independent, identically distributed Gaussian fluctuations of the two pump beams, the OPAs operate at 1% of oscillation threshold on average, 2 dB/km fiber loss, 5 dB excess loss in each source-to-memory link, and source-to-memory path length L = 25 km.

Figure 7 examines the throughput and fidelity behavior for two cases of detuning errors. There are six frequencies involved in our teleportation architecture: ω_S and ω_I, the center frequencies of the signal and idler beams from the dual-OPA source; $\omega_P = \omega_S + \omega_I$, the dual-OPA's pump frequency; ω_C, the resonant frequency of the memory cavities; ω_A, the 795-nm-wavelength line of the trapped Rb atoms; and Γ, the linewidth of the dual-OPA source. In Case 1 of Fig. 7 we assume that the dual-OPA source is detuned by $\Delta\omega$ from frequency degeneracy $\omega_P/2$, and that this degeneracy point coincides with both the memory cavity resonance and the atomic line. In Case 2 of Fig. 7 we assume that the dual-OPA source operates at degeneracy, but that $\omega_P/2$ is detuned by $\Delta\omega$ from $\omega_C = \omega_A$. We see from Fig. 7 that detuning errors have a disastrous effect on throughput if they are in excess of the dual-OPA's linewidth, but do not cause a problem with fidelity.

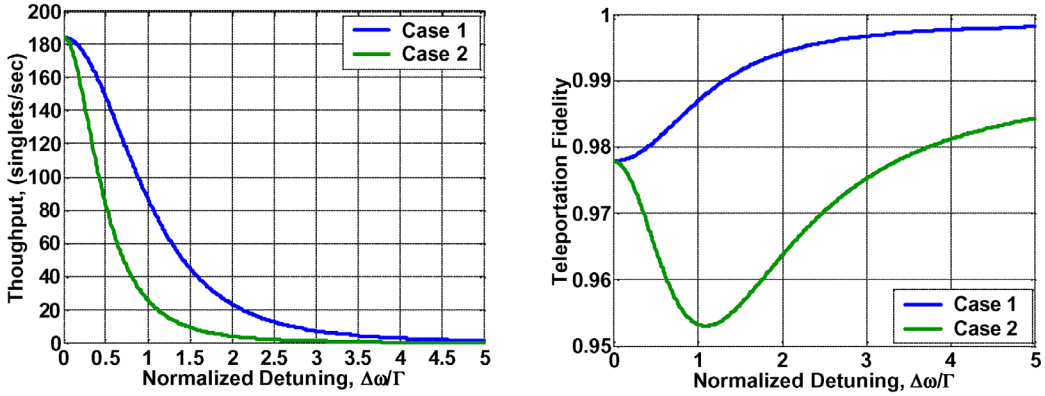

Figure 7. Left: throughput versus normalized detuning. Right: teleportation fidelity versus normalized detuning. Case 1 assumes that the signal and idler center frequencies are detuned from degeneracy, with the degeneracy point matched to the memory cavity resonance and the atomic line. Case 2 assumes that the dual-OPA operates at frequency degeneracy, but the degeneracy point is detuned from the memory cavity resonance, which we take to be the same as the atomic line. The rest of the parameters are the same as those used in Fig. 4.

Dual-Beam High-Flux Polarization Entanglement Source In recent years most entanglement sources are based on spontaneous parametric downconversion (SPDC) in a noncollinearly propagating, angle phase-matched crystal, such as beta barium borate (BBO) [8]. We have recently taken a different approach to entanglement generation that is based on periodically-poled potassium titanyl phosphate (PPKTP) with collinear propagation of the pump, signal, and idler fields. In a single-beam configuration we have previously obtained very good results: 99% quantum-intereference visibility with a coincidence flux of 300/s/mW of pump power. We have also measured the Clauser, Horne, Shimony, and Holt (CHSH) form of Bell's inequality violation [9] showing a value of 2.711 ± 0.017 [10]. However, in both noncollinear and collinear configurations, spatial filtering (aperture), spectral filtering (interference filter), and temporal filtering (timing compensating crystal) are necessary for generating polarization entanglement at the expense of significantly reduced flux. Recently we have taken a dual-beam approach to generating polarization-entangled photons at high flux without the need for spatial, spectral, and temporal filtering [11]. We have achieved a record coincidence flux of 12,000/s/mW of pump power, a factor of more than ten higher than any bulk-crystal entanglement source.

We have implemented the dual-beam downconverter in Fig. 8 using a 10-mm-long hydrothermally-grown PPKTP crystal with a grating period of 9.01 μm that is designed for frequency-degenerate type-II quasi-phase matched operation at a pump wavelength of 397 nm. The PPKTP crystal is pumped bidirectionally along the crystal's *x*-axis with a single pump source, thus effectively creating two identical coherently pumped downconverters. We rotate the outputs

of one of the beams by 90° and combine the two downconverted beams at a polarizing beam splitter, whose outputs are polarization entangled independent of the output frequencies and propagation directions. We have effectively engineered a decoherence-free subspace in which all output photon pairs are polarization entangled. There is complete indistinguishability (spatially, spectrally, and temporally) at the output, so that it is impossible to tell which downconverter a photon comes from, and hence it must be a coherent superposition of the two downconverted beams [4].

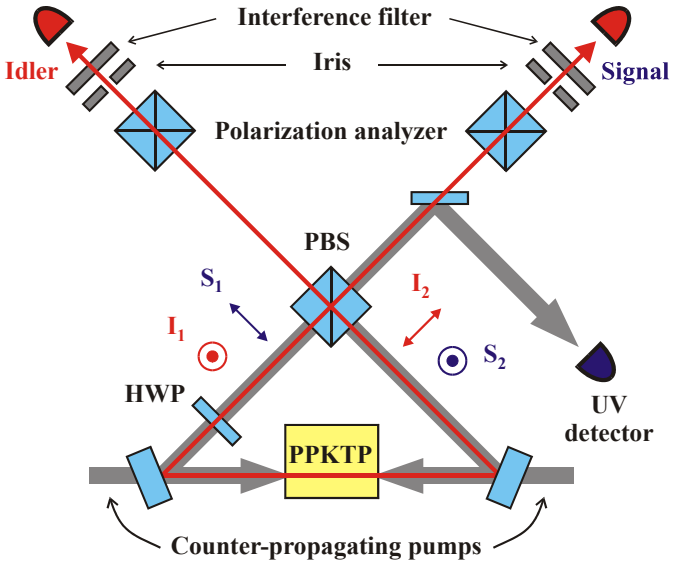

Figure 8. Schematic of dual-beam downconverter setup. The PBS combines the two downconverted outputs to form polarization-entangled signal and idler beams, which may have different wavelengths. UV detector monitors the pump interferometer phase. HWP, half-wave plate; PBS, polarizing beam splitter.

The state of the polarization-entangled output is given by

$$|\psi\rangle = \left(|H\rangle_1|V\rangle_2 - e^{i\phi}|V\rangle_1|H\rangle_2\right)/\sqrt{2},$$

where the phase ϕ is equal to the pump interferometer phase ϕ_p, plus a fixed offset phase that is related to material dispersion of the interferometer. The interferometer is formed by the 50-50 beam splitter used for bidirectional pumping and the output polarizing beam splitter shown in Fig. 8. As a result, the state of the output can be precisely controlled by locking the classical pump interferometer at a fixed pump phase position. In Fig. 9, the coincidence counts are shown as a function of time when the pump phase is locked for maximum or minimum count rates, indicating the stable control of the output state over time.

Figure 10 shows the quantum interference results of our dual-beam entanglement source. The main plot displays the quantum-interference visibility as a function of the diameter of an iris that is used as a spatial filter. As the iris diameter increases, we observe a slow drop of the visibility at a rate that is much smaller than that in the single-beam downconversion configuration [10], as expected. The small drop in visibility is caused by internal clipping of the output field before their combination at the polarizing beam splitter. The left inset plots the flux as a function of the iris aperture size, indicating a very high flux level that results from the dual-pump configuration. In the right inset the visibility is plotted versus the signal and idler wavelengths, showing that the visibility has no wavelength dependence.

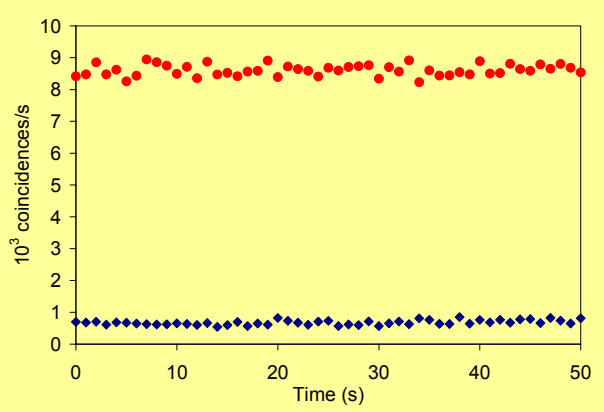

Figure 9. Coincidence rate versus time for pump-phase locked dual-beam downconverter. Red (blue): pump phase is locked for maximizing (minimizing) coincidence count rate.

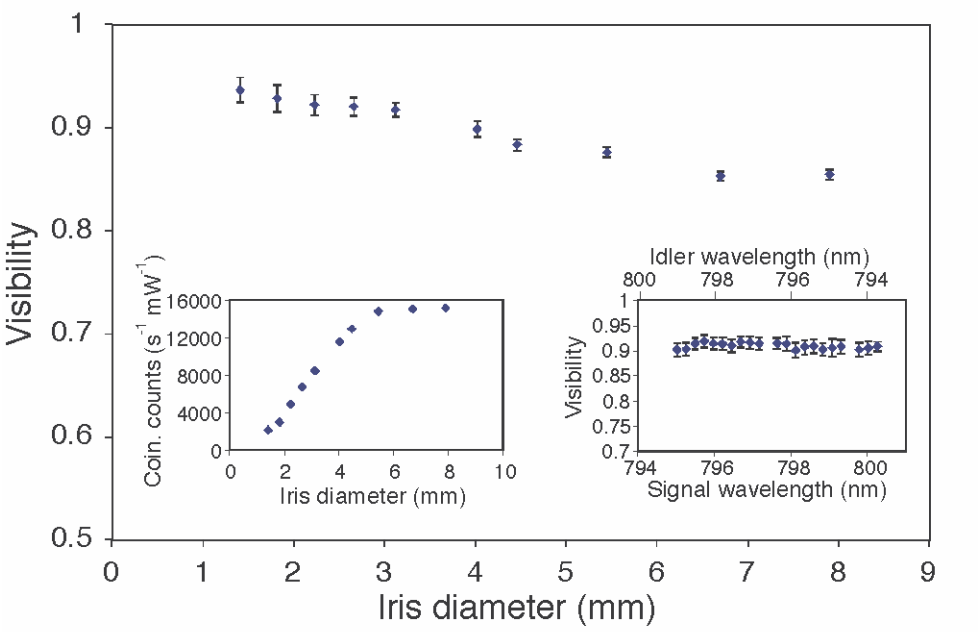

Figure 10. Plot of quantum-interference visibility and coincidence flux (left inset) as a function of aperture diameter for interference filter bandwidth of 3 nm. Right inset: visibility as a function of signal and idler wavelengths, measured with no interference filter.

High-Flux Source of Highly Nondegenerate Polarization-Entangled Photon Pairs We have recently demonstrated an efficient periodically-poled lithium niobate (PPLN) parametric downconverter with collinearly propagating outputs of highly nondegenerate photon pairs [12]. For the generation of polarization entanglement from a type I phase matched system such as PPLN, it is necessary to use a dual-pump configuration, as shown in Fig. 11. The co-polarized outputs at ~800 nm and ~1600 nm are separated with a prism and the two downconverted beams are combined to yield the two polarization-entangled output beams, similar to our PPKTP bidirectional pumping configuration. The output photons are fiber coupled for easy transport and analysis. Polarization entanglement coincidence measurements of the two output beams are shown in Fig. 12, indicating a strong quantum correlation. We measure the CHSH form of Bell's inequality violation yielding an *S* parameter of 2.606 ± 0.010.

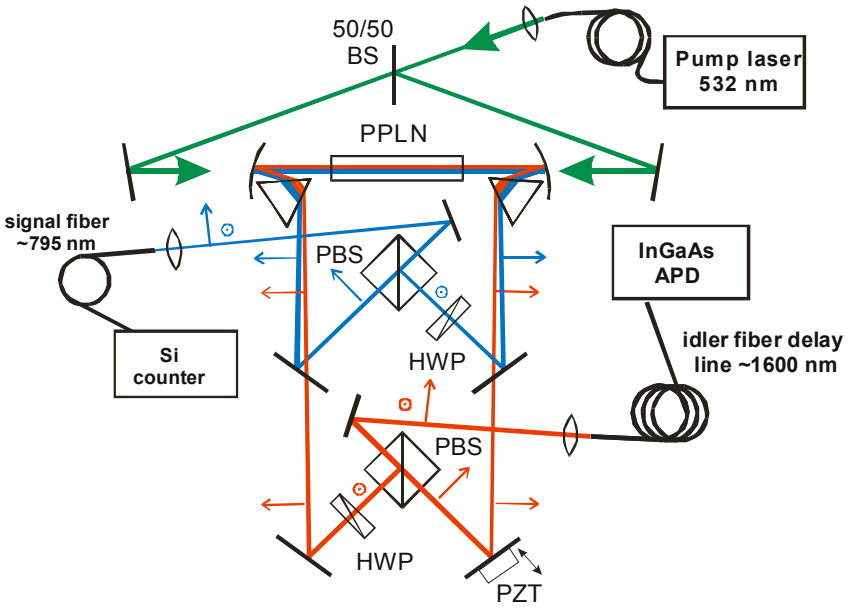

Figure 11. Schematic of dual-pump PPLN downconverter experimental setup. Signal (blue) and idler (red) are spectrally separated by prisms, and the PBS combines the two downconverted outputs of each color to form polarization-entangled signal and idler beams. HWP, half-wave plate; PBS, polarizing beam splitter; BS, beam splitter; PZT, piezoelectric transducer.

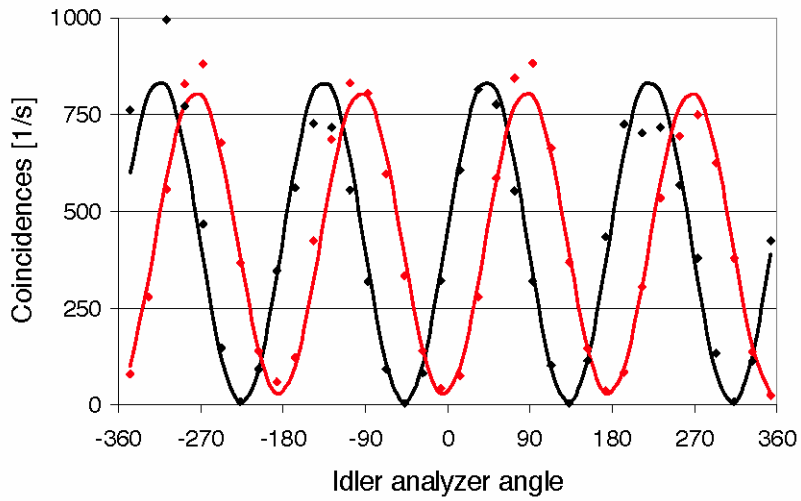

Figure 12. Plots of coincidence counts for signal analyzer angles of 0° (black) and 45° (red) as functions of the idler analyzer angle.

The PPLN entanglement source is particularly useful for implementing the MIT/NU long-distance quantum teleportation protocol [1]. In this protocol, the 795-nm output is for loading a local trapped-Rb quantum memory, and the ~1600-nm output is transmitted through an optical fiber and then frequency translated to 795 nm for loading a remotely located trapped-Rb quantum memory. Typical bandwidths for a trapped Rb atom in a high-finesse optical cavity are tens of MHz, and most SPDC entanglement sources have spectral brightness that is too low for quantum memory loading applications. Our PPLN source, on the other hand, is suitable for initial testing in narrowband applications. We have measured the spectral bandwidth of our fiber-coupled source

to be ~60 GHz. Based on our measured pair generation flux, we estimate that our fiber-coupled source has a flux of 10/s/mW of pump within a 30-MHz bandwidth. We project that by switching to a first-order PPLN grating (instead of the third-order grating in the present setup) and a 100-mW pump, we should be able to generate ~10,000 entangled pairs/s within a narrow bandwidth of 30 MHz. The wide tunability, high efficiency, and narrow bandwidth of this PPLN source make it useful for many other quantum entanglement applications.

Efficient Single-Photon Upconversion at 1550 nm The MIT/NU long-distance teleportation protocol depends on efficient frequency translation of a photonic quantum state at ~1600 nm, used for long-distance fiber optic transmission, to one at 795 nm, used to load the trapped-Rb quantum memory. We have recently demonstrated a first step toward single-photon quantum state translation by efficiently upconverting continuous-wave (cw) light at 1550 nm to 631 nm at the single photon level. Based on efficient three-wave mixing in a 4-cm-long PPLN crystal, this upconverter mixes a photon at 1554 nm with a strong pump field at 1064 nm, converting the 1554 nm photon to 631 nm with 90% efficiency [13]. A ring cavity for the 1064-nm pump produces a circulating power of ~23 W from an input of ~400 mW. The PPLN crystal is temperature stabilized at ~200°C for optimal phase matching of the three interacting wavelengths. We attenuate a 1554-nm laser to a level of 0.09 photon/μs for input into the upconverter, and the upconverted light is detected using a Si avalanche photodiode single-photon counter. The upconversion results are shown in Fig. 13, with single-photon efficiency reaching 90% at a pump level of 22 W. We have also observed a significant level of background counts that is due to the upconversion of pump-induced fluorescence photons with the same spectral and spatial properties as the input light at 1554 nm [13]. For coincidence measurements the background counts are not a serious problem. In order to eliminate them completely, it is necessary to curb the generation of pump-induced fluorescence, such as by pumping the upconverter at a wavelength that is longer than that of the input photon.

As an efficient single-photon counter for 1550-nm photons, our upconversion system demonstrates high efficiency in continuous-wave operation with no after-pulsing. For quantum-state frequency translation, it is necessary to preserve the polarization state of the photon. Because PPLN upconversion is polarization selective, additional effort — such as polarization separation followed by two-channel upconversion and interferometric recombination — is needed for efficient polarization-insensitive upconversion. Such a device would be of considerable value in a number of classical and quantum applications.

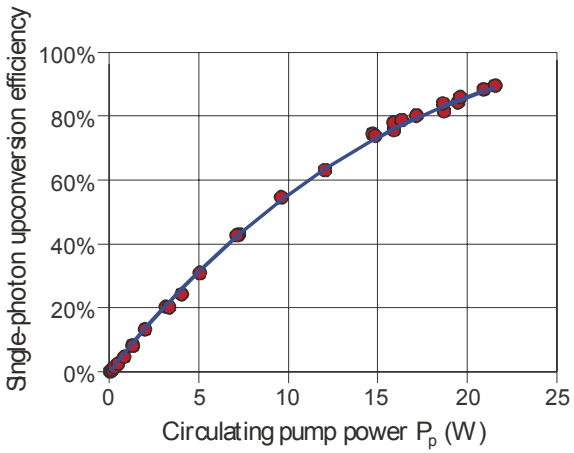

Figure 13. Single-photon upconversion efficiency as a function of circulating pump power at 1064 nm.

Classical Capacity of Free-Space Optical Communication A principal goal of quantum information theory is evaluating the information capacities of important communication channels. At present — despite the many efforts that have been devoted to this endeavor [14] — exact

capacity results are known for only a handful of channels. Recently, we have begun addressing this capacity problem for a broad class of bosonic channels, viz., those involving loss and thermal noise. The basic construct starts from the Holevo-Schumacher-Westmoreland theorem [15,16], which states that the classical capacity of a quantum channel characterized by a completely-positive (CP) map *E* is given by

$$C = \sup_n \left(C_n / n \right)$$

where

$$C_n = \max_{p_j, \sigma_j} \chi\left(p_j, E^{\otimes n}\left[\sigma_j \right] \right)$$

is the capacity achieved in *n* channel uses, $\{p_j\}$, $\{\sigma_j\}$ are, respectively, the sets of prior probabilities and input density operators for the information symbols $\{j\}$, and

$$\chi\left(p_j, \sigma_j \right) = S\left(\sum_j p_j \sigma_j \right) - \sum_j p_j S\left(\sigma_j \right)$$

defines the Holevo information χ in terms of the von Neumann entropy *S*. The supremum in this capacity development in necessitated by the fact that Holevo information may be superadditive.

Our primary interest lies in bosonic channels [17-22], specifically those associated with free-space propagation [18-20], but we have also addressed waveguide propagation [17]. Prior to our efforts, the major extant capacity result was for lossless — and hence noiseless — propagation [23,24]. In this case, transmitted states arrive undisturbed at the receiver. For a single-mode electromagnetic field that is subject to an average photon-number constraint *N*, the resulting capacity in bits per channel use — realized by a random coding ensemble over photon number states in conjunction with photon-counting reception — is then

$$C = g(N) \equiv (N+1)\log_2(N+1) - N\log_2(N).$$

The corresponding capacity for wideband operation under an average power constraint *P* is

$$C = \frac{1}{\ln(2)} \sqrt{\frac{\pi P}{3\hbar}}\, T,$$

where *T* is the signaling time. Once again, random coding over photon-number states together with photon-counting reception is used to achieve capacity.

We have derived narrowband and wideband capacity results for the pure-loss bosonic channel, in which the propagation loss — channel transmissivity $\eta<1$ — is accompanied by the minimal amount of quantum noise (vacuum-state quantum noise) that is required by quantum mechanics [18]. It turns out that the Holevo information is not superadditive for this channel, and random coding over coherent states achieves capacity. The resulting capacity formulas are identical to those given for the lossless channel with *N* replaced by ηN in the single-mode case, and *P* replaced by ηP in the wideband case with frequency-independent loss. Interestingly, because our results also apply to the lossless case, $\eta=1$, we have a coherent-state route to achieving capacity on this channel. Conversely, photon-number states do not achieve capacity over the pure-loss channel when $\eta<1$.

Frequency-independent loss makes for a simple wideband capacity formula, but it does not represent the wideband behavior of free-space optical communications. For far-field line-of-sight propagation over an L-m-long path between circular apertures of areas A_t and A_r, we have obtained the capacity curves shown in Fig. 14 for optimum reception, heterodyne detection, and homodyne detection [18,19]. As suggested by the figure, heterodyne detection is asymptotically optimum at high average power levels.

In addition to the pure-loss channel, in which only vacuum-state quantum noise is injected, we have made substantial progress toward establishing capacity results for two other important channels. The first is the thermal-noise channel, in which loss is accompanied by injection of quantum noise from an isotropic mixture of coherent states. The second is the classical-noise channel, in which classical isotropic Gaussian noise is added to an otherwise lossless channel. The latter models a lossy channel with post-propagation optical amplification used to offset the loss. We have developed reasonably tight lower and upper bounds on the capacity of these channels [20,21]. These bounds are consistent with the conjecture that capacity is achieved — for the thermal-noise and classical-noise channels — by coherent-state encoding as in the pure-loss case. That conjecture would be proven if we could show that coherent-state inputs minimize the output von Neumann entropy for these channels. Minimum output entropy is an important problem in its own right, and we have made significant headway toward a proof of this property [21,22]. As shown in Fig. 15, we have reasonably tight lower and upper bounds on the minimum entropy. We have also shown that coherent-state inputs minimize integer-order Rényi and Wehrl entropies at the outputs of these channels.

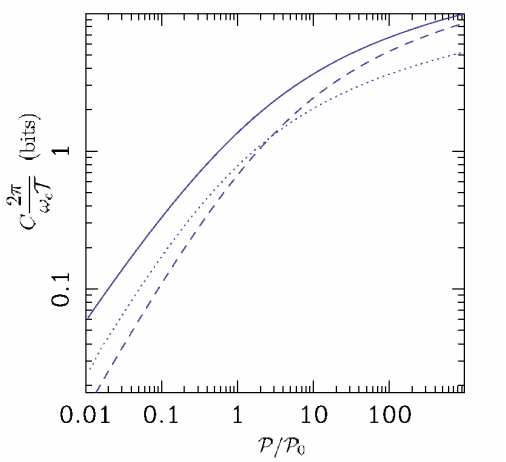

Figure 14. Capacities of the far-field free-space optical channel as a function of the input power P [in this plot, $P_0 = 2\pi\hbar c^2 L^2 / A_t A_r$]. The solid curve is the capacity C; the other two curves are the information rates achievable with coherent states and heterodyne detection (dashed curve) or coherent states and homodyne detection (dotted curve). Note that the heterodyne detection performance approaches capacity in the high-power limit.

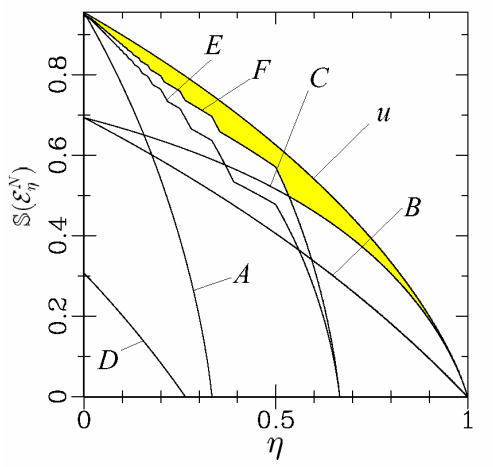

Figure 15. Bounds on the minimum output entropy of the thermal-noise channel as functions of the channel transmissivity η for average thermal photon number 1/2. Curves *A*, *B*, *C*, *D*, *E*, and *F* are all lower bounds. Curve *u* is the upper bound, $g((1-\eta)/2)$, which is also our conjectured minimum output entropy for this case.

2. Atmospheric Optical Communications

Sponsor
Defense Advanced Research Projects Agency - Grant MD1972-00-1-0012

Project Staff
Professor Jeffrey H. Shapiro, Dr. Franco N. C. Wong, Baris I. Erkmen, Mohsen Razavi

In future battlefield operations, communications and data networking will play a much more significant role. Properly designed optical communication systems operating over atmospheric paths may be able to provide covert, high burst rate communications with the necessary quick set up and tear down capability. Laser beams propagating through the atmosphere are subject to a wide variety of deleterious effects, including absorption, depolarization, beam spread, angular spread, multipath spread, Doppler spread, and fading. These effects, which represent the combined impact of the atmosphere's molecular constituents, entrained aerosols and hydrometeors, and turbulence-induced refractive index fluctuations, may drastically curtail the performance of an atmospheric optical link. We are working, in collaboration with Professor Vincent Chan of the Laboratory for Information and Decision Systems, to: provide understanding of battlefield optical communication applications and their implied demands on optical systems; develop architectural constructs that are attainable, but make maximum use of device and subsystem capability to achieve high overall performance; and develop and demonstrate key system concepts in an experimental test bed facility.

The central focus of this program is to address the effects of atmospheric turbulence and how it may be mitigated through the use of diversity techniques in space, time, and frequency. Our work in this regard includes both theoretical and experimental efforts. In previous work we have studied coding [25,26] and capacity [26-28] for the multiple-input, multiple-output (MIMO) optical communication channel shown schematically in Fig. 16. We have also analyzed the use of spatial diversity reception — without multiple transmitters — together with optical preamplification as a means for reducing the ill effects of turbulence-induced scintillation [29,30]. Here we have considered a suite of possible receivers, as shown in Fig. 17. During the past year, however, our theory effort has concentrated on near-field communication performance [31,32], while our experimental work has continued to explore various approaches to communication diversity.

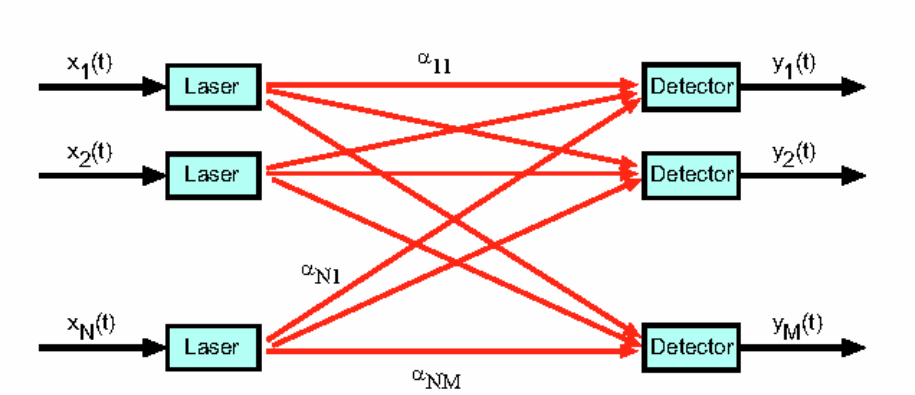

Figure 16. Block diagram of the multiple-input, multiple-output, single-user channel with turbulence-induced fading. A single-user information source modulates *N* laser sources. These lasers couple to *M* photodetectors via independent, identically distributed path gains.

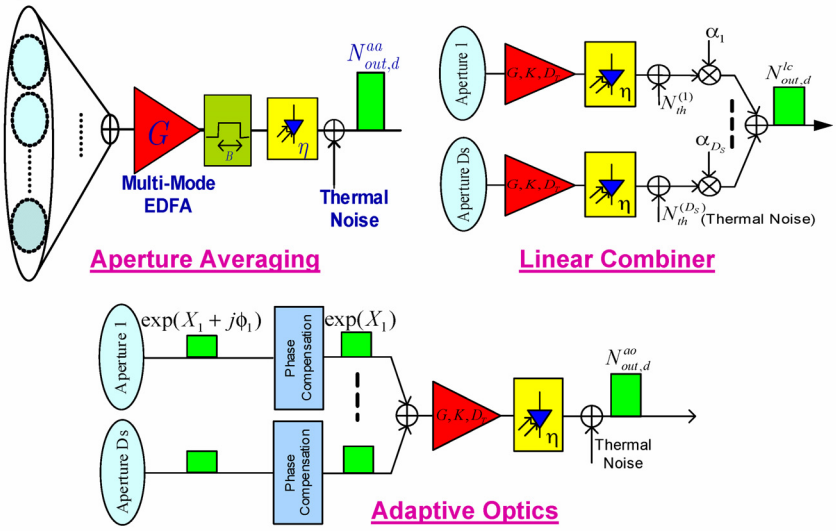

Figure 17. Three classes of direct-detection diversity receivers, all using erbium-doped fiber amplifiers (EDFAs). In each case the receiver aperture consists of multiple atmospheric-turbulence coherence areas. The aperture averaging receiver combines the light from all of these coherence areas on a multi-mode EDFA prior to direct detection. The linear combiner uses a single-mode EDFA (gain *G*, noise factor *K*, and D_T temporal modes) for each coherence area followed by direct detection, and weighted linear combining. The adaptive optics receiver first compensates for the turbulence-induced phase differences between the coherence areas, permitting the use of a single-mode EDFA prior to direct detection. All three receivers are subject to post-detection additive thermal noise.

Almost all previous work on line-of-sight atmospheric optical communications presumes far-field propagation models, in which the transmitted beam is much larger than the receiver aperture. However, with the availability of steered agile-beam technology, it may become practical to operate in the near-field regime, wherein active tracking is used to maintain alignment between a transmitter beam that is smaller than the receiver aperture. Although a good deal is known about imaging in near-field operation, very little has been done about its communication possibilities. Near-field operation offers potential advantages with respect to low-probability of intercept and low-probability of detection. We have therefore been working to derive (or bound) the fading

statistics incurred in near-field operation, and use these results to study the error probability performance in near-field communication [31,32]. The left and right panels of Fig. 18 show, respectively, the worst-case (maximum error probability) and best-case (minimum error probability) near-field fading distributions that are consistent with fractional power transfer through turbulence with mean 0.99 and variance 0.005. Figure 19 shows the corresponding densities when an additional unimodality constraint is enforced. Figure 20 shows the beta distribution, a unimodal distribution on the interval [0,1], with mean 0.99 and variance 0.005. We have used the probability densities from Figs. 18-20 to obtain bounds on the error probability of on-off-keyed coherent detection and direct detection near-field systems. Our error probability results are shown in Figs. 21 and 22. These figures show that the bounds we have obtained can be quite loose, for coherent detection, and that the beta distribution gives performance that approximates that of the worst-case unimodal distribution. Note that because the direct detection receiver we have considered in Fig. 22 does not employ optical preamplification, its sensitivity is substantially inferior to the coherent detection system.

We have also studied the ergodic and outage capacities of near-field communications through atmospheric turbulence. Our work on near-field capacity has been limited, however, to the case of coherent (heterodyne) detection. For the ergodic capacity we have shown that

$$2\overline{\eta}W\log_2\left(1+\frac{P}{2N_0W}\right)\le C_E\le 2W\log_2\left(1+\frac{\overline{\eta}P}{2N_0W}\right)$$

where $\overline{\eta}$ is the average of the maximum power-transfer eigenvalue for the near-field communication scenario. Inasmuch as $\overline{\eta}\approx 1$ prevails when the free-space Fresnel number product of the transmitter and receiver apertures is much greater than unity, this result shows that turbulence has virtually no effect on near-field channel capacity with coherent detection.

Figure 18. Left: worst-case (maximum error probability) near-field fading distribution. Right: best case (minimum error probability) near-field fading distribution. Both distributions assume a 0.99 mean and a 0.005 variance for the fractional power transfer.

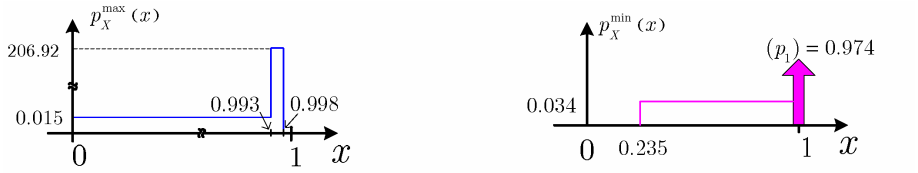

Figure 19. Left: worst-case (maximum error probability) near-field fading distribution. Right: best case (minimum error probability) near-field fading distribution. Both distributions assume a 0.99 mean and a 0.005 variance for the fractional power transfer, and both distributions are unimodal.

We set up an OC-24 (1.2-Gb/s) open-air link between a laboratory on the 4th floor of Building 35 and the roof of Building N10, spanning an effective path length of ~250 m. A cw laser at one of the ITU grid wavelengths (~1559 nm) is externally modulated with a bias-free modulator before being launched into free space with a 10x telescope. The output power is adjustable with the use of a variable fiber-optic attenuator located after the modulator. A high-quality 20-cm-diameter flat high reflector is mounted on a mirror mount inside a wooden box that is securely situated on the roof of Building N10. The transmitted light is reflected at the rooftop mirror back to the laboratory

for detection. We estimate that the return beam has a beam diameter of ~25 cm. Portions of the returned light are collected by two optical diversity receivers that are spatially separated by 18 cm to ensure low correlations in turbulence-induced fading.

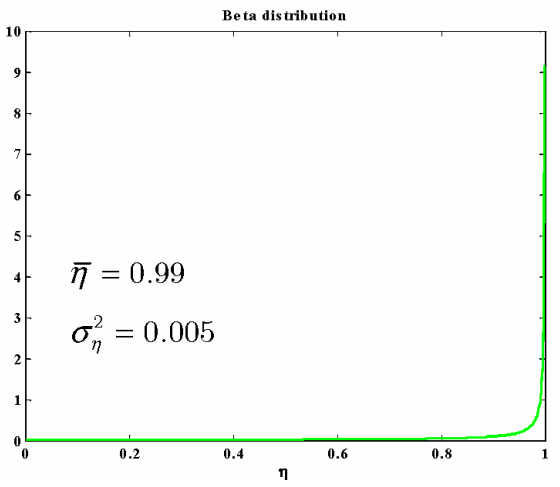

Figure 20. Beta distribution for fractional power transfer; mean 0.99 and variance 0.005 assumed.

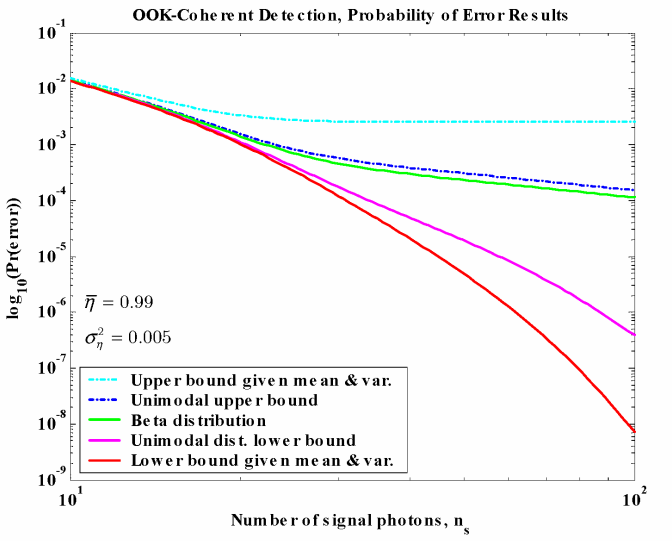

Figure 21. On-off-keying (OOK) error probability bounds for near-field coherent detection. The OOK error probability for beta-distribution fading is also shown. All curves assume a fractional power transfer with mean 0.99 and variance 0.005.

Figure 23 shows the components of one of the two optical receivers. A 2.5-cm-diameter lens with a focal length of 10 cm is used to focus the incoming light, which is approximately flattop within the lens aperture, into a single-mode optical fiber. For output power of 2 dBm, we typically capture about -37 dBm per receiver. The receiver signal is then optically amplified with an erbium doped fiber amplifier (EDFA) to boost its signal strength, narrowband filtered to reduce the amplified spontaneous emission noise from the EDFA, and detected using a *p-i-n* photodiode. The two resultant electrical signals from the diversity receivers are amplified, low-pass filtered, and combined with equal weight for bit-error rate analysis. We also monitored the detected

power levels at the *p-i-n* diode detectors to record the fluctuations at the input aperture of the two optical receivers. We have observed that the fading statistics are largely uncorrelated. We have evaluated the performance of the two-receiver diversity reception system and significant improvement has been observed with the system compared with a single receiver. The improvement in bit-error rates is due partly to the collection of twice the optical power of a single receiver. It is also partly a result of the compensating capability of diversity reception systems, in which uncorrelated mild fading at the two receiver apertures has a low probability of simultaneous loss of signal in both channels. Figure 24 shows plots of the measured bit-error rates as a function of the single-receiver power and the theoretical curves corresponding to the measured fading statistics. The plots clearly show the advantages of the 2-receiver diversity scheme and the relatively close fit between experiment and theory.

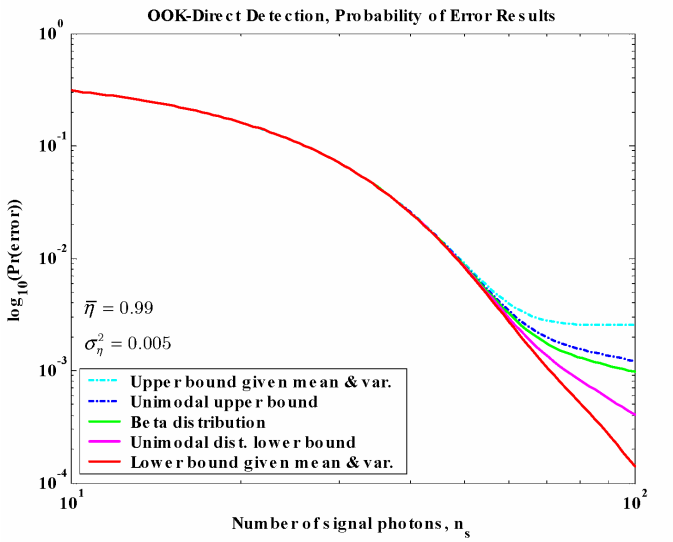

Figure 22. On-off-keying (OOK) error probability bounds for near-field direct detection. The OOK error probability for beta-distribution fading is also shown. All curves assume a fractional power transfer with mean 0.99 and variance 0.005.

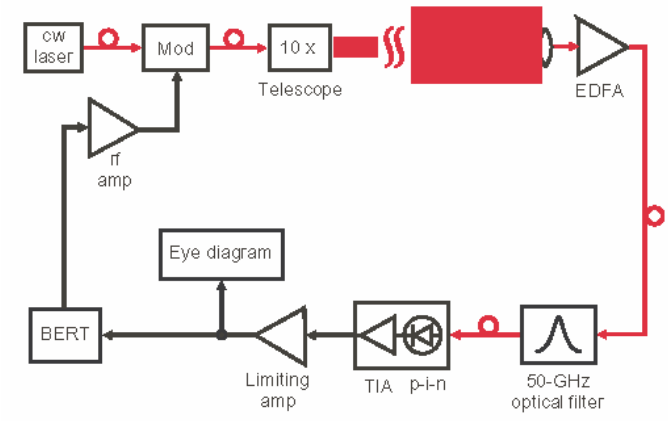

Figure 23. Schematic of 1.2-Gb/s free-space link. Mod: OOK modulator; EDFA: erbium-doped fiber amplifier; TIA: transimpedance amplifier; BERT: bit error rate tester.

We have also explored the use of wavelength diversity, as a route to mitigating turbulence-induced fading. Rytov-approximation (weak perturbation) propagation theory suggests that

wavelength diversity will not be effective, i.e., the wavelength separation that is necessary for multiple transmitters to encounter independent scintillation is an appreciable fraction of their nominal wavelength [33]. To our knowledge, however, this assertion has not been studied in a high-data-rate communication test bed such as ours. In our experiment, lasers operating at 1559 nm (channel #1) and 1546 nm (channel #2) were modulated with a common 1.2 Gb/s data stream, combined through a fused fiber coupler, and sent over our 250-m-long atmospheric path. At the receiver we used a single telescope and EDFA. The two wavelengths were selected by narrowband filters and routed to a pair of photodetectors. This operating arrangement ensures that the only diversity advantage that could accrue here is due to wavelength separation, i.e., both channels share the same transmitter and receiver apertures. Figure 25 shows histograms of the log-power distributions (normalized to have zero means) on each channel taken in light turbulence conditions. These figures also fit the log-power histograms to Gaussian distributions, which is equivalent to fitting the power fading to the lognormal distribution expected in the weak perturbation regime. Figure 26 shows the correlation coefficient between the two channels. This figure clearly indicates that our 13-nm wavelength separation provides no useful diversity.

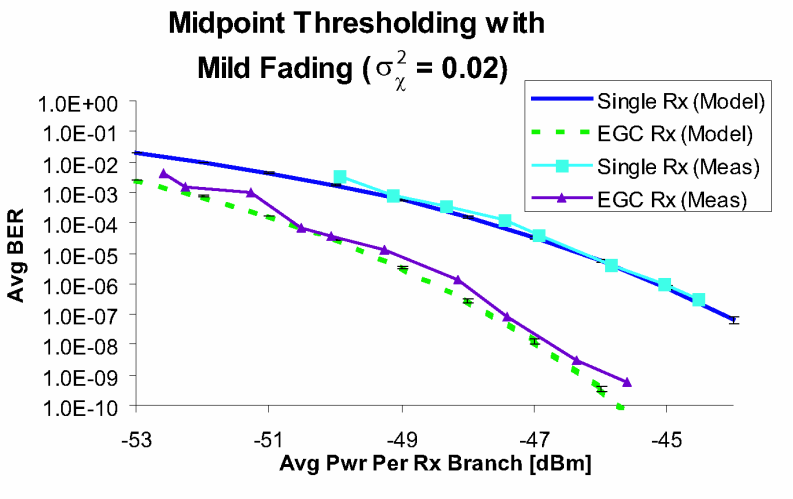

Figure 24. Bit error rate (BER) measurements versus received optical power at the input of EDFA for single receiver and equal-gain-combining (EGC) two-receiver diversity reception. Also shown are theoretical error probability results, based on our system calibration and the measured logamplitude variance.

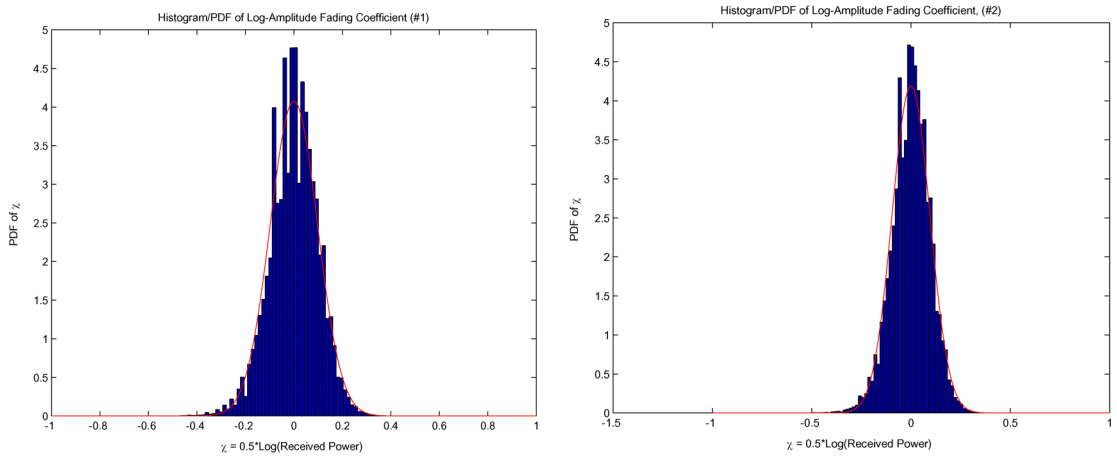

Figure 25. Histograms of log-received power for light turbulence conditions. Left: channel #1 (1559 nm wavelength). Right: channel #2 (1546 nm wavelength).

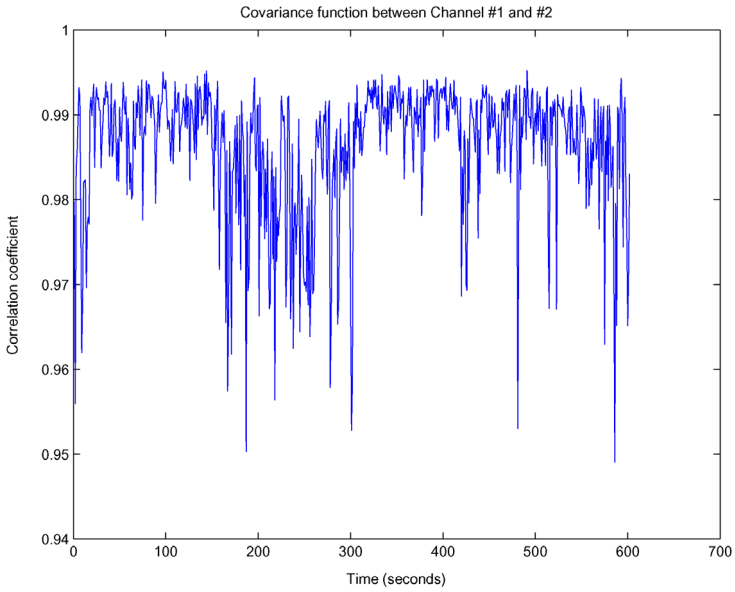

Figure 26. Log-received power correlation coefficient for the scintillation data shown in Fig. 25.

References

1. J. H. Shapiro, "Architectures for Long-Distance Quantum Communication," *New J. Phys*. 4, 47.1-47.18 (2002).

2. C. H. Bennett, G. Brassard, C. Crépeau, R. Jozsa, A. Peres, and W. K. Wootters, "Teleporting and Unknown Quantum State via Dual Classical and Einstein-Podolsky-Rosen Channels," *Phys. Rev. Lett*. 70, 1895-1899 (1993).

3. S. Lloyd, M. S. Shahriar, J. H. Shapiro, and P. R. Hemmer, "Long-Distance Unconditional Teleportation of Atomic States via Complete Bell State Measurements," *Phys. Rev. Lett*. 87, 167903 (2001).

4. J. H. Shapiro and N. C. Wong, "An Ultrabright Narrowband Source of Polarization-Entangled Photon Pairs," *J. Opt. B: Quantum Semiclass*. *Opt*. 2, L1-L4 (2000).

5. J. Aung, *Quantum Error Modeling and Correction in Long Distance Teleportation using Singlet States*, S.M. thesis, Department of Electrical Engineering and Computer Science, MIT, 2002.

6. J. H. Shapiro, J. Aung, and B. J. Yen, "Quantum Error Models and Error Mitigation for Long-Distance Teleportation Architectures," *Proceedings of the Feynman Festival*, College Park, MD, August 2002, quant-ph/0211086.

7. B. J. Yen and J. H. Shapiro, "Error Models for Long-Distance Qubit Teleportation," IEEE *J. Sel. Topics in Quantum Electron*. 9, 1483-1494 (2003).

8. P. G. Kwiat, E. Waks, A. G. White, I. Appelbaum, and P. H. Eberhard, "Ultrabright Source of Polarization-Entangled Photons," *Phys. Rev. A* 60, R773-R776 (1999).

9. J. F. Clauser, M. A. Horne, A. Shimony, and R. A. Holt, "Proposed Experiment to Test Local Hidden-Variable Theories," *Phys. Rev. Lett.* 23, 880-884 (1969).

10. C. E. Kuklewicz, M. Fiorentino, G. Messin, F. N. C. Wong, and J. H. Shapiro, "High-Flux Source of Polarization-Entangled Photons from a Periodically Poled $KTiOPO_4$ Parametric Down-Converter," *Phys. Rev. A* 69, 013807 (2004).

11. M. Fiorentino, G. Messin, C. E. Kuklewicz, F. N. C. Wong, and J. H. Shapiro, "Generation of Ultrabright Tunable Polarization Entanglement without Spatial, Spectral or Temporal Constraints," *Phys. Rev. A* 69, 041801(R) (2004).

12. E. J. Mason, M. A. Albota, F. König, and F. N. C. Wong, "Efficient Generation of Tunable Photon Pairs at 0.8 and 1.6 μm," *Opt. Lett*. 27, 2115-2117 (2002).

13. M. A. Albota and F. N. C. Wong, "Efficient Single-Photon Counting at 1.55 μm by means of Frequency Upconversion," *Opt. Lett*., forthcoming.

14. C. H. Bennett and P. W. Shor, "Quantum Information Theory," *IEEE Trans. Information Theory* 44, 2724-2742 (1998), and references therein.

15. A. S. Holevo, "The Capacity of the Quantum Channel with General Signal States," *IEEE Trans. Information Theory* 44, 269-273 (1998).

16. B. Schumacher and M. D. Westmoreland, "Sending Classical Information via Noisy Quantum Channels," *Phys. Rev. A* 56, 131-138 (1997).

17. V. Giovannetti, S. Lloyd, L. Maccone, and J. H. Shapiro, "Information Rate of a Waveguide," *Phys. Rev. A*, forthcoming; e-print quant-ph/0307112.

18. V. Giovannetti, S. Guha, S. Lloyd, L. Maccone, J. H. Shapiro, and H. P. Yuen, "Classical Capacity of the Lossy Bosonic Channel: the Exact Solution," *Phys. Rev. Lett*. 92, 027902 (2004).

19. S. Guha, *Classical Capacity of the Lossy Bosonic Far-Field Channel*, S.M. thesis, Department of Electrical Engineering and Computer Science, MIT 2004.

20. J. H. Shapiro, V. Giovannetti, S. Guha, L. Maccone, and H. P. Yuen, "Classical Capacity of Free-Space Optical Communication," to appear in *60th Birthday Volume in Honor of Alexander S. Holevo*, ed. O. Hirota (Rinton Press, 2004).

21. V. Giovannetti, S. Guha, S. Lloyd, L. Maccone, and J. H. Shapiro, "Minimum Output Entropy of Bosonic Channels: a Conjecture," *Phys. Rev. A*, forthcoming; e-print quant-ph/0404005.

22. V. Giovannetti, S. Lloyd, L. Maccone, J. H. Shapiro, and B. J. Yen, "Minimum Rényi and Wehrl Entropies at the Output of Bosonic Channels," *Phys. Rev. A*, forthcoming; e-print quant-ph/0404037.

23. H. P. Yuen and M. Ozawa, "Ultimate Information Carrying Limit of Quantum Systems," *Phys. Rev. Lett*. 70, 363-366 (1993).

24. C. M. Caves and P. D. Drummond, "Quantum Limits on Bosonic Communication Rates," Rev. Mod. Phys. 66, 481-537 (1994).

25. S. M. Haas, J. H. Shapiro, and V. Tarokh, "Space-Time Codes for Wireless Optical Communications," *EURASIP J. Appl. Signal Process*. 3, 211-220 (2002).

26. S. M. Haas, *Capacity and Coding for Multiple-Aperture, Wireless, Optical Communications*, Ph.D. thesis, Department of Electrical Engineering and Computer Science, MIT 2003.

27. S. M. Haas and J. H. Shapiro, "Capacity of the Multiple-Input, Multiple-Output Poisson Channel," in B. Pasik-Duncan, ed*., Stochastic Theory and Control, Proceedings of a Workshop held in Lawrence, Kansas, October 18-20, 2001* (Springer-Verlag, Berlin, 2002).

28. S. M. Haas and J. H. Shapiro, "Capacity of Wireless Optical Communications*," IEEE J. Sel. Areas in Commun*. 21, 1346-1357 (2003).

29. M. Razavi and J. H. Shapiro, "Wireless Optical Communications via Diversity Reception and Optical Preamplification," *Proceedings of the IEEE International Conference on Communications*, Anchorage, Alaska, May 11-15, 2003.

30. M. Razavi and J. H. Shapiro, "Wireless Optical Communications via Diversity Reception and Optical Preamplification," *IEEE Trans. on Wireless Commun*., forthcoming.

31. B. I. Erkmen, *Performance analysis for near-field atmospheric optical communications*, M.Eng. thesis, Department of Electrical Engineering and Computer Science, MIT, 2003.

32. B. I. Erkmen and J. H. Shapiro, "Performance analysis for near-field atmospheric optical communications," submitted to the IEEE 2004 Global Telecommunications Conference, Dallas, Texas, November 29- December 3, 2004.

33. A. Ishimaru, *Wave Propagation and Scattering in Random Media, Vol. 2* (Academic Press, New York, 1978), Chap. 19.

Publications

Journal Articles, Published

J. H. Shapiro, "Near-Field Turbulence Effects on Quantum Key Distribution," *Phys. Rev. A* 67, 022309 (2003).

C.-P. Yeang, C. Cho, and J. H. Shapiro, "A Target-Recognition Theory of SAR Imagery using Electromagnetics-Based Signatures," *Opt. Engr*. 42, 2129-2149 (2003).

S. M. Haas and J. H. Shapiro, "Capacity of Wireless Optical Communications*," IEEE J. Sel. Areas in Commun*. 21, 1346-1357 (2003).

B. J. Yen and J. H. Shapiro, "Error Models for Long-Distance Qubit Teleportation," *IEEE J. Sel. Topics in Quantum Electron*. 9, 1483-1494 (2003).

V. Giovannetti, S. Guha, S. Lloyd, L. Maccone, J. H. Shapiro, and H. P. Yuen, "Classical Capacity of the Lossy Bosonic Channel: the Exact Solution," *Phys. Rev. Lett*. 92, 027902 (2004).

C. E. Kuklewicz, M. Fiorentino, G. Messin, F. N. C. Wong, and J. H. Shapiro, "High-Flux Source of Polarization-Entangled Photons from a Periodically Poled $KTiOPO_4$ Parametric Down-Converter," *Phys. Rev. A* 69, 013807 (2004).

F. König and F. N. C. Wong, "Extended Phase Matching of Second-Harmonic Generation in Periodically Poled $KTiOPO_4$ with Zero Group-Velocity Mismatch," *Appl. Phys. Lett.* 84, 1644 (2004).

M. Fiorentino, G. Messin, C. E. Kuklewicz, F. N. C. Wong, and J. H. Shapiro, "Generation of Ultrabright Tunable Polarization Entanglement without Spatial, Spectral or Temporal Constraints," *Phys. Rev. A* 69, 041801(R) (2004).

Journal Articles, Accepted for Publication

M. Razavi and J. H. Shapiro, "Wireless Optical Communications via Diversity Reception and Optical Preamplification," *IEEE Trans. on Wireless Commun.*, forthcoming.

V. Giovannetti, S. Lloyd, L. Maccone, and J. H. Shapiro, "Information Rate of a Waveguide," *Phys. Rev. A*, forthcoming.

V. Giovannetti, S. Guha, S. Lloyd, L. Maccone, and J. H. Shapiro, "Minimum Output Entropy of Bosonic Channels: a Conjecture," *Phys. Rev. A*, forthcoming.

V. Giovannetti, S. Lloyd, L. Maccone, J. H. Shapiro, and B. J. Yen, "Minimum Rényi and Wehrl Entropies at the Output of Bosonic Channels," *Phys. Rev. A*, forthcoming.

M. A. Albota and F. N. C. Wong, "Efficient Single-Photon Counting at 1.55 μm by means of Frequency Upconversion," *Opt. Lett.*, forthcoming.

J.-J. Zondy, D. Kolker, and F. N. C. Wong, "Dynamical Signatures of Self Phase-Locking in a Triply Resonant Optical Parametric Oscillator," *Phys. Rev. Lett.*, forthcoming.

Journal Articles, Submitted for Publication

V. Giovannetti, S. Lloyd, L. Maccone, J. H. Shapiro, and F. N. C. Wong, "Conveyor Belt Clock Synchronization," submitted to *Phys. Rev. A*.

M. Fiorentino and F. N. C. Wong, "Deterministic Controlled-NOT Gate for Single-Photon Two-Qubit Quantum Logic," submitted to *Phys. Rev. Lett*.

P. Kumar, P. Kwiat, A. Migdall, S. W. Nam, J. Vuckovic, and F. N. C. Wong, "Photonic Technologies for Quantum Information Processing," submitted to *Quantum Inf. Proc*.

T. Kim, M. Fiorentino, P. V. Gorelik, and F. N. C. Wong, "Low-Cost Nanosecond Electronic Coincidence Detector," submitted to *Rev. Sci. Instrum*.

O. D. Mucke, O. Kuzucu, F. N. C. Wong, E. P. Ippen, F. X. Kaertner, S. M. Foreman, D. J. Jones, L.-S. Ma, J. L. Hall, and J. Ye, "Experimental Implementation of Optical Clockwork without Carrier-Envelope Phase Control," submitted to *Opt. Lett*.

Books/Chapters in Books

J. H. Shapiro and O. Hirota, eds., *Proceedings of the Sixth International Conference on Quantum Communication, Measurement and Computing* (Rinton Press, Princeton, 2003).

D. Abbott, J. H. Shapiro, and Y. Yamamoto, eds., *Fluctuations and Noise in Photonics and Quantum Optics, Proc. SPIE vol. 5111* (SPIE, Bellingham, 2003).

J. H. Shapiro, V. Giovannetti, S. Guha, L. Maccone, and H. P. Yuen, "Classical Capacity of Free-Space Optical Communication," to appear in *60th Birthday Volume in Honor of Alexander S. Holevo*, ed. O. Hirota (Rinton Press, 2004).

Meeting Papers, Presented

F. König, E. J. Mason, F. N. C. Wong, and M. A. Albota, "Efficient Generation of Polarization-Entangled Photon Pairs at 795 and 1610 nm," paper presented at the 4th European Quantum Information Processing and Communication Workshop, Oxford, United Kingdom, July 13-18, 2003.
J. H. Shapiro, F. N. C. Wong, P. Kumar, and M. S. Shahriar, "Progress towards Long-Distance, High-Fidelity Quantum Teleportation, paper presented at the Annual Meeting of the Optical Society of America, Tucson, Arizona, October 5-9, 2003.

Meeting Papers, Published

M. Razavi and J. H. Shapiro, "Wireless Optical Communications via Diversity Reception and Optical Preamplification," *Proceedings of the IEEE International Conference on Communications*, Anchorage, Alaska, May 11-15, 2003.

J. H. Shapiro, "Quantum Gaussian Noise," *Proc. SPIE* 5111, 382-395 (2003).

B. J. Yen and J. H. Shapiro, "Error Models and Error Mitigation for Long-Distance, High-Fidelity Quantum Secret Sharing, *Proc. SPIE* 5111, 104-107 (2003).

C. E. Kuklewicz, G. Messin, F. N. C. Wong, and J. H. Shapiro, "Generation of Polarization Entanglement from a PPKTP Parametric Downconverter," *Digest of Quantum Electronics and Laser Science Conference*, Baltimore, Maryland, June 1-6, 2003.

M. Fiorentino, C. E. Kuklewicz, G. Messin, F. N. C. Wong, and J. H. Shapiro, "Ultrabright Tunable Photon-Pair Source with Total-Flux Polarization Entanglement," *Digest of Quantum Electronics and Laser Science Conference*, Baltimore, Maryland, June 1-6, 2003.

M. Fiorentino, G. Messin, C. E. Kuklewicz, F. N. C. Wong, and J. H. Shapiro, "Ultrabright Tunable Photon-Pair Source with Total-Flux Polarization-Entanglement," *Digest of Quantum Electronics and Laser Science Conference*, Baltimore, MD, June 1-6 2003, Postdeadline paper QThPDB2.

M. A. Albota and F. N. C. Wong, "Efficient Single-Photon Counting at 1.55 μm via Frequency Upconversion," *Digest of Quantum Electronics and Laser Science Conference*, Baltimore, MD, June 1-6 2003, Postdeadline paper QThPDB11.

M. Fiorentino and F. N. C. Wong, "Deterministic Controlled-NOT Gate for Two-Qubit Single-Photon Quantum Logic," *Digest of International Conference on Quantum Electronics*, San Francisco, California, May 22-27 2004.

J.-J. Zondy, D. Kolker, and F. N. C. Wong, "Dynamical Signature of Self Phase-Locking in a Triply Resonant Parametric Oscillator," *Digest of Conference on Lasers and Electro-Optics*, San Francisco, California, May 22-27 2004.

F. N. C. Wong, M. A. Albota, and J. H. Shapiro, "Quantum Frequency Translation: Efficient Photon Counting at 1.55 μm," *Digest of International Conference on Quantum Electronics*, San Francisco, California, May 22-27, 2004.

O. D. Muecke, O. Kuzucu, N. C. Wong, E. P. Ippen, F. X. Kaertner, S. M. Foreman, D. J. Jones, L.-S. Ma, J. L. Hall, and J. Ye, "Experimental Implementation of Optical Clockwork without Carrier-Envelope Phase Control," *Digest of Conference on Lasers and Electro-Optics*, San Francisco, California, May 22-27 2004, Postdeadline paper CPDC9.

M. Fiorentino, T. Kim, and F. N. C. Wong, “Entanglement Swapping in a Single-Photon Two-Qubit Logic Circuit,” *Digest of International Conference on Quantum Electronics*, San Francisco, California, May 22-27 2004, Postdeadline paper IPDA11.

Theses

B. I. Erkmen, *Performance analysis for near-field atmospheric optical communications*, M.Eng. thesis, Department of Electrical Engineering and Computer Science, MIT, 2003.

S. Guha, *Classical Capacity of the Lossy Bosonic Far-Field Channel*, S.M. thesis, Department of Electrical Engineering and Computer Science, MIT 2004.